Magnetic Properties of [FeFe]-Hydrogenases: A Theoretical Investigation Based on Extended QM and QM/MM Models of the H-Cluster and Its Surroundings

Greco, Claudio; Silakov, Alexey; Bruschi, Maurizio; Ryde, Ulf; De Gioia, Luca; Lubitz, Wolfgang

Published in:
European Journal of Inorganic Chemistry

DOI:
10.1002/ejic.201001058

2011

Document Version:
Peer reviewed version (aka post-print)

DOI: 10.1002/ejic.200((will be filled in by the editorial staff))

Magnetic properties of [FeFe]-hydrogenases: a theoretical investigation based on extended QM and QM/MM models of the H-cluster and its surroundings

Claudio Greco*,[a] Alexey Silakov*,[b] Maurizio Bruschi,[c] Ulf Ryde,[d] Luca De Gioia[a] and Wolfgang Lubitz[b]

Keywords: [FeFe]-hydrogenases / Density Functional Theory / EPR parameters calculation / Quantum Mechanics – Molecular Mechanics

In the present contribution, we report a theoretical investigation of the magnetic properties of the dihydrogen-evolving enzyme [FeFe]-hydrogenase, based on both DFT models of the active site (the H-cluster, a Fe_6S_6 assembly including a binuclear portion directly involved in substrates binding) and QM/MM models of the whole enzyme. Antiferromagnetic coupling within the H-cluster has been treated using the broken-symmetry approach, along with the use of different density functionals. Results of *g*-value calculations turned out to largely vary as a function of the level of theory and of the extension of the model. The choice of the broken-symmetry coupling scheme also had a large influence on the calculated *g* values and such instabilities were observed for both the active–ready (H_{ox}) and the CO-inhibited (H_{ox}-CO) enzyme forms. However, hyperfine coupling-constant calculations were found to provide more stable and consistent results. This allowed us to show that the experimentally detected delocalization of an unpaired electron at the binuclear subcluster in *Desulfovibrio desulfuricans* H_{ox} is compatible with a weak interaction between the catalytic centre and a water molecule.

[a] Department, Institution, Address 1
Fax: Fax number
E-mail: E-mail address
[b] Max Planck Institute for Bioinorganic Chemistry,.
45468 Mülheim and der Ruhr, Stiftstrasse 34-36, Germany
Fax: +49 (208) 3063951
E-mail: A.S.: silakov@mpi-muelheim.mpg.de
[c]
[d]

Supporting information for this article is available on the WWW under http://www.eurjic.org/ or from the author. ((Please delete if not appropriate.))

Introduction

[FeFe]-hydrogenases are dihydrogen-evolving/oxidising enzymes that possess a peculiar Fe_6S_6 complex in their active site (the "H-cluster", see Figure 1). The key steps underlying catalysis take place at a specific binuclear portion of the H-cluster. This binuclear subcluster, generally referred to as $[2Fe]_H$, is linked to the remaining tetranuclear portion of the active site (which will be referred to as the $[4Fe\text{-}4S]_H$ subcluster) by means of a cysteine sulphur atom (S_1 in Figure 1).

The disclosure of the H-cluster structural features by means of X-ray crystallography has allowed researchers to investigate the enzyme structure in detail.[1-4] In this context, spectroscopic investigations based on IR absorption deepened our insights of the peculiar coordination environment of metal centres **Xxx The paper was a mixture of US and UK English. I have assumed UK, because it is a European Journal.** in the $[2Fe]_H$ subcluster:[5-7] The latter features the biologically unusual presence of cyanide and carbonyl ligands. One of the CO groups turned out to be in bridging position between the two iron atoms in all the enzymatic states, except for the completely reduced enzyme, in which it moves to a terminal position.[4, 7] The H-cluster can attain different redox states: The partially oxidised, CO-bridged form is able to perform H_2 uptake, and it features a paramagnetic, mixed-valence Fe(I)Fe(II) redox state at the $[2Fe]_H$ subsite,[8, 9] while the $[4Fe\text{-}4S]_H$ subcluster attains the 2Fe(II)2Fe(III) state.[9, 10] This form of the H-cluster, usually referred to as "H_{ox}", is thought to bind exogenous H_2 at the vacant coordination site indicated by an arrow in Fig. 1 (this iron ion is termed "distal", Fe_d, while the second metal ion in the subcluster is termed "proximal", Fe_p, based on their relative positions with respect to the tetranuclear portion of the H-cluster).[4, 11, 12] Notably, the Fe_d centre in H_{ox} can also bind exogenous CO, giving rise to the CO-inhibited form of the enzyme, H_{ox}-CO.[3, 6, 13, 14] Single-electron reduction of H_{ox} yields the reduced, H_{red} form of the active site, which is able to bind protons, thus starting the catalytic process of H_2 evolution.[9, 12, 15] H_{red} is a diamagnetic state of the H-cluster, attaining the Fe(I)Fe(I) and 2Fe(II)2Fe(III) states of the $[2Fe]_H$ and $[4Fe\text{-}4S]_H$ subclusters, respectively.[9]

In the present paper, which is focussed on the magnetic properties of the H-cluster, we present for the first time theoretical results on the EPR parameters and hyperfine couplings of the entire H-cluster in the paramagnetic forms H_{ox} and H_{ox}-CO. The models are geometry-optimized using density functional theory (DFT), and the environment of the H-cluster is represented by using either a continuum solvent model (COSMO)[16] or by means of an explicit all-atom representation of the protein matrix based on molecular mechanics (MM). The results are compared with those obtained using simple Fe_2S_2 models of the isolated $[2Fe]_H$ subcluster.[14, 17-19]

As noted in previous studies, reproduction of the experimental EPR *g* factors and hyperfine couplings of hydrogenases is challenging.[14, 17-20] In particular, previous theoretical studies based on simple models of the $[2Fe]_H$ subsite gave only partially satisfactory results for the H_{ox} and H_{ox}-CO states.[14, 17-19] This might be due to one or more of the following reasons: (i) models of the isolated $[2Fe]_H$ subcluster completely neglect the electronic effects of the $[4Fe\text{-}4S]_H$ subcluster, which are thought to play a relevant role in the [FeFe]-hydrogenase chemistry;[15, 21, 22] (ii) a poor reproduction of the environment of the H-cluster might

prevent the fine reproduction of the geometrical and electronic features of the latter, thus affecting the quality of the magnetic properties calculations;[18, 21] (iii) from a methodological point of view, the accuracy of electron densities obtained by DFT methods is also a matter of concern for the calculation of magnetic properties; (iv) finally, the possible presence of labile ligands such as metal-bound water molecules might deeply affect the H-cluster electron density, a point that has not been thoroughly investigated. The above issues have been tackled in the present paper, by performing magnetic properties computation at different levels of theory and by including in the models the effects of the $[4Fe\text{-}4S]_H$ subsite and of the surrounding protein matrix. The antiferromagnetic coupling characterizing the $[4Fe\text{-}4S]_H$ subcluster was treated using the broken-symmetry (BS) approach,[23] which is based on localizing opposite spins on selected Fe_2S_2 layers composing the tetranuclear H-cluster subsite.[15, 19] [add Greco et al., International Journal of Quantum Chemistry, accepted] The possibility that a water ligand might be bound to the distal iron atom in H_{ox} was taken into account as well.

Results and Discussion

1. H_{ox}-CO models. The calculated hyperfine couplings and *g* factors for the H_{ox}-CO form of the enzyme are reported in Table 1. Let us first analyze the isolated Fe_6S_6 models, optimized in the COSMO continuum solvent. Two models were considered: **1-$Fe_6S_6^{BS1}$** and model **1-$Fe_6S_6^{BS2}$**, Figure 2. These models differ in terms of broken-symmetry coupling scheme (as described in Methods). A comparison between the experimental *g* factors of *Desulfovibrio desulfuricans* hydrogenase (DdH) (g_1 = 2.00; g_2 = 2.01; g_3 = 2.07)[21] and theoretical B3LYP results for **1-$Fe_6S_6^{BS1}$** (g_1 = 1.98, g_2 = 2.02, g_3 = 2.06) shows that g_2 and g_3 are better reproduced than g_1. However, the BS1 state is significantly less stable than the alternative BS2 state (ΔE = 12 kJ/mol), and switching to the latter wavefunction leads to a large change in the computed g_2 and g_3 values, so that g_3 becomes as low as 2.03, while g_2 is now smaller by 0.02. This illustrates that the choice of BS solutions is non-innocent in terms of *g* factors calculations, a point that will apply to most of the calculations in the present paper.

Removing the Fe_4S_4 cluster from the model (**1-$Fe_2S_2^{TRUNC}$**, obtained by truncation of **1-$Fe_6S_6^{BS1}$**) leads to a large change in the computed *g* values (g_1 = 2.01, g_2 = 2.02, g_3 = 2.03). Now, the two theoretical *g* values that better reproduce the corresponding experimental values are g_1 and g_2. In fact, the difference between theory and experiment for g_3 is as large as 0.04; notice also that the *g* factors calculated for **1-$Fe_2S_2^{TRUNC}$** are essentially indistinguishable from those previously obtained by Brunold et al. on Fe_2S_2 models truncated by the inclusion of a $SHCH_3$ moiety and geometry-optimized using the BP86 functional and the zeroth-order regular approximation (ZORA) Hamiltonian (in that case, the *g* values calculated with ORCA were the following: g_1 = 2.01, g_2 = 2.02, g_3 = 2.03).[19] The inclusion in the QM model of the protein portion in the immediate neighbourhood of the $[2Fe]_H$ cluster (**1-Fe_2S_2_surr**) leads to a picture close to the one already described for **1-$Fe_2S_2^{TRUNC}$** (see Table 1). On the contrary, optimization of the H-cluster in an all-atom representation of the whole DdH enzyme (model **1-DdH$^{QM/MM}$**, see Methods) leads to computed *g* factors that are closer to experiment: g_1 = 1.99, g_2 = 2.01, g_3 = 2.05. The maximum difference between these *g* factors and experimental data is 0.02 (for g_3).

As for the choice of the density functional for H-cluster *g* factors calculations, B3LYP results tend to show an overall smaller divergence from the experimental results for the considered models, but the consistency and stability of computed *g* values appear to be larger in the case of BP86 functional (see Table 2).

Finally, hyperfine couplings of the Fe_p and Fe_d centres and of the carbon atom of the Fe_d-bound exogenous CO group have also been computed. It turned out that they are generally overestimated (see Table 1, where the corresponding experimental values for DdH are reported as well).[21] For example, while the experimental hyperfine couplings in DdH turned out to be 4 and 1 MHz for the Fe_p and Fe_d centres, respectively, the corresponding computed values for the enzyme model **1-DdH$^{QM/MM}$** are as large as 22 and 12 MHz in the case of B3LYP models. In other words, the theoretical couplings of Fe_p and Fe_d are approximately 5–12 times too large compared to the experimental data, indicating that the spin excess on the metal centres is overestimated in the model. Very similar conclusions can be drawn for the C atom of the exogenous carbonyl ligand (the calculated value for **1-DdH$^{QM/MM}$** was 54 MHz, compared to the experimental value of 17 MHz). Notably, an analogous hyperfine coupling was previously obtained by B3LYP computations on binuclear H-cluster models truncated by a CH_3S^- fragment).[19] Overestimation of the hyperfine couplings was observed for the BP86 results as well (Table 2). However, in this case a notable result is obtained: The ratio between experimental couplings for Fe_p and Fe_d in DdH (4.0/0.8 = 5) is in reasonable agreement with theory (ratios around 3 and 4.2 for **1-DdH$^{QM/MM}$** and **1-$Fe_2S_2^{TRUNC}$**, respectively; see Table 2). For the ratio between the hyperfine couplings of the Fe_p centre and the C atom of the exogenous CO ligand, the experimental and computational values are again not too far from each other (experimental ratio 0.23; calculated ratios 0.30 and 0.48 for models **DdH$^{QM/MM}$** and **1-$Fe_2S_2^{TRUNC}$**, respectively; Table 2). Notice that the computed couplings do not vary appreciably when going from binuclear to hexanuclear models. This is because the extension of the QM representation to the entire H-cluster does not cause any redistribution of spin over the atoms composing the model (see spin population of the Fe_p and Fe_d centres in Table 1 and 2).

2. H_{ox} models. Let us now analyze the H_{ox} state of the enzyme. We have investigated models showing a vacant coordination site on Fe_d first (see models of **2** type in Figure 2). The COSMO-optimized Fe_6S_6 model of the isolated H-cluster **2-$Fe_6S_6^{BS1}$** gives g_1 = 2.03, g_2 = 2.06, g_3 = 2.10 (Table 3, B3LYP results). These computed EPR parameters qualitatively reproduce the general features of the experimental spectrum for the partially oxidized DdH enzyme: g_1 = 2.00, g_2 = 2.04, g_3 = 2.10. However, a quite different set of computed *g* factors is obtained when the spin-density pattern at the $[4Fe\text{-}4S]_H$ subcluster is changed: the model **2-$Fe_6S_6^{BS2}$** gives: g_1 = 1.97, g_2 = 2.05, g_3 = 2.09, meaning that the difference between the computed *g* factors in the two electronic states can be as large as 0.06. The **2-$Fe_6S_6^{BS2}$** *g* values are overall in worse agreement with the experimental data, but notice that **2-$Fe_6S_6^{BS2}$** shows negligible stability difference with **2-$Fe_6S_6^{BS1}$** ($\Delta E_{BS1-BS2}$ = 3 kJ/mol). In this context, it is worth noting that an average set of *g* values obtained from the two BS states (g_1 = 2.00, g_2 = 2.06, g_3 = 2.10) is closer to the experimental results, compared to the *g* values of the models considered separately. Such average set of *g* factors is also similar to the *g* values calculated for the truncated Fe_2S_2 model **2-$Fe_2S_2^{TRUNC}$** (g_1 = 2.01, g_2 = 2.05, g_3 = 2.09). The extended **2-Fe_2S_2_surr** model gives theoretical *g* factors similar to those of the naked Fe_2S_2 model (g_1 = 2.01, g_2 = 2.06, g_3 = 2.09, Table 3). On the other hand, the QM/MM model **2-DdH$^{QM/MM}$** gives computed *g* factors rather far from the experimental values (g_1 = 2.04, g_2 = 2.07, g_3 = 2.09). However, truncation of the QM/MM optimized H-cluster to a $[2Fe]_H$ model gives *g* factors (g_1 = 2.01, g_2 = 2.05, g_3 = 2.09), that are the same as those computed for **2-$Fe_2S_2^{TRUNC}$**. Notice that the *g* values for the truncated models are close to the theoretical values reported by Brunold et al. (g_1 = 2.01, g_2 = 2.04, g_3 = 2.08).[19] Finally, the BP86 method reproduce the experimental g_1 value better than B3LYP, but the opposite is found for g_3 (see Table 4).

For the hyperfine couplings, calculated Fe_p couplings turned out to be too low in all models, while the opposite is true for Fe_d. This applied to both B3LYP (Table 3) and BP86 (Table 4). A most

important difference is that in the experiment, equal hyperfine couplings were found for the proximal and the distal iron, while in the calculations, the coupling are about one order of magnitude different.

3. H_{ox}-H_2O models. Finally, we consider H_{ox} models with a labile water ligand bound to the Fe_d centre (model of the **3** type, see Figure S2 in Supplementary Information). In this case, all the investigated Fe_2S_2 and Fe_6S_6 models give *g* factors that do not satisfactory fit the experimental data, with deviations equal to or larger than 0.03 for one or more of the *g* factors (B3LYP results, see Table 5). In particular, as far as constrained Fe_6S_6 models are concerned, the BS2 state, which is more stable than the BS1 model ($\Delta E_{BS1-BS2}$ = 23 kJ/mol), gives B3LYP *g* values (g_1 = 1.97, g_2 = 2.03, g_3 = 2.06, Table 5) that are far from experiments. The BP86 functional also fails to reproduce the experimental *g* values (see Table 6). **Xxx Perhaps you should turn this down somewhat: The errors are not larger than in other studies, especially as you later argue that this is the preferred model.**
On the other hand, the calculated Fe_p and Fe_d hyperfine couplings turned out to be closer to the experimental values, compared to those obtained for models with a vacant coordination site on Fe_d. In any case, the B3LYP hyperfine couplings are systematically overestimated by a factor up to 2, as shown in Table 5, while those computed at BP86 level for the water-bound adducts are even closer to the experimental results (see Table 6).

Table 1. *g* factors, hyperfine couplings and Mulliken spin populations calculated at the B3LYP/TZVP level on H_{ox}-CO models **1**. Experimental data are also included.[21]

Model Name	*g* factors	Hyperfine couplings (MHz)	Mulliken spin pop.
1-$Fe_6S_6^{BS1}$	g_1 = 1.98 g_2 = 2.02 g_3 = 2.06	Fe_p = 22.92 Fe_d = 12.97 C_{exg} = 51.88	Fe_p = 0.45 Fe_d = 0.37
1-$Fe_6S_6^{BS2}$	g_1 = 1.98 g_2 = 2.00 g_3 = 2.03	Fe_p = 22.04 Fe_d = 11.92 C_{exg} = 49.27	Fe_p = 0.47 Fe_d = 0.35
1-$Fe_2S_2^{TRUNC}$	g_1 = 2.01 g_2 = 2.02 g_3 = 2.03	Fe_p = 29.13 Fe_d = 9.98 C_{exg} = 38.17	Fe_p = 0.59 Fe_d = 0.29
1-Fe_2S_2_surr	g_1 = 2.01 g_2 = 2.01 g_3 = 2.02	Fe_p = 25.10 Fe_d = 11.32 C_{exg} = 38.17	Fe_p = 0.53 Fe_d = 0.33
1-$DdH^{QM/MM}$	g_1 = 1.99 g_2 = 2.01 g_3 = 2.05	Fe_p = 22.54 Fe_d = 12.14 C_{exg} = 54.28	Fe_p = 0.50 Fe_d = 0.36
Exp.	g_1 = 2.00 g_2 = 2.01 g_3 = 2.07	Fe_p = 4.0 Fe_d = 0.8 C_{exg} = 17.1	- - -

Table 2. *g* factors, hyperfine couplings and Mulliken spin populations calculated at the BP86/TZVP level on H_{ox}-CO models **1**. Experimental data are also included.[21]

Model Name	*g* factors	Hyperfine couplings (MHz)	Mulliken spin pop.
1-$Fe_6S_6^{BS1}$	g_1 = 1.97 g_2 = 2.02 g_3 = 2.02	Fe_p = 20.73 Fe_d = 7.65 C_{exg} = 67.51	Fe_p = 0.50 Fe_d = 0.27
1-$Fe_6S_6^{BS2}$	g_1 = 1.99 g_2 = 2.01 g_3 = 2.04	Fe_p = 18.10 Fe_d = 6.31 C_{exg} = 58.58	Fe_p = 0.43 Fe_d = 0.23
1-$Fe_2S_2^{TRUNC}$	g_1 = 2.00 g_2 = 2.01 g_3 = 2.02	Fe_p = 26.91 Fe_d = 6.42 C_{exg} = 56.09	Fe_p = 0.58 Fe_d = 0.23
1-Fe_2S_2_surr	g_1 = 2.00 g_2 = 2.01 g_3 = 2.02	Fe_p = 22.88 Fe_d = 7.08 C_{exg} = 63.86	Fe_p = 0.54 Fe_d = 0.26
1-$DdH^{QM/MM}$	g_1 = 1.99 g_2 = 2.01 g_3 = 2.02	Fe_p = 20.37 Fe_d = 6.88 C_{exg} = 67.50	Fe_p = 0.51 Fe_d = 0.26
Exp.	g_1 = 2.00 g_2 = 2.01 g_3 = 2.07	Fe_p = 4.0 Fe_d = 0.8 C_{exg} = 17.1	- - -

Table 3. *g* factors, hyperfine couplings and Mulliken spin populations calculated at the B3LYP/TZVP level on H_{ox} models **2**. Experimental data are also included.[21]

Model Name	*g* factors	Hyperfine couplings (MHz)	Mulliken spin pop.
2-$Fe_6S_6^{BS1}$	g_1 = 2.03 g_2 = 2.06 g_3 = 2.10	Fe_p = 2.02 Fe_d = 32.88	Fe_p = 0.13 Fe_d =1.07
2-$Fe_6S_6^{BS2}$	g_1 = 1.97 g_2 = 2.05 g_3 = 2.09	Fe_p = 0.09 Fe_d = 32.59	Fe_p = 0.10 Fe_d = 1.04
2-$Fe_2S_2^{TRUNC}$	g_1 = 2.01 g_2 = 2.05 g_3 = 2.09	Fe_p = 0.39 Fe_d = 31.84	Fe_p = 0.10 Fe_d = 1.05
2-Fe_2S_2_surr	g_1 = 2.01 g_2 = 2.06 g_3 = 2.09	Fe_p = 2.33 Fe_d = 31.84	Fe_p = 0.14 Fe_d = 0.96
2-$DdH^{QM/MM}$	g_1 = 2.04 g_2 = 2.07 g_3 = 2.09	Fe_p = 3.12 Fe_d = 34.95	Fe_p = 0.15 Fe_d = 1.14
Exp.	g_1 = 2.00 g_2 = 2.04 g_3 = 2.10	Fe_p = 12.4 Fe_d = 12.4	- -

Table 4. *g* factors, hyperfine couplings and Mulliken spin populations calculated at the BP86/TZVP level on H_{ox} models **2**. Experimental data are also included.[21]

Model Name	*g* factors	Hyperfine couplings (MHz)	Mulliken spin pop.
2-$Fe_6S_6^{BS1}$	$g_1 = 2.00$ $g_2 = 2.03$ $g_3 = 2.07$	$Fe_p = 2.94$ $Fe_d = 25.32$	$Fe_p = 0.18$ $Fe_d = 0.91$
2-$Fe_6S_6^{BS2}$	$g_1 = 2.00$ $g_2 = 2.04$ $g_3 = 2.07$	$Fe_p = 0.62$ $Fe_d = 24.26$	$Fe_p = 0.14$ $Fe_d = 0.86$
2-$Fe_2S_2^{TRUNC}$	$g_1 = 2.01$ $g_2 = 2.03$ $g_3 = 2.06$	$Fe_p = 1.16$ $Fe_d = 24.98$	$Fe_p = 0.14$ $Fe_d = 0.91$
2-Fe_2S_2_surr	$g_1 = 2.01$ $g_2 = 2.04$ $g_3 = 2.06$	$Fe_p = 2.50$ $Fe_d = 27.43$	$Fe_p = 0.17$ $Fe_d = 0.84$
2-$DdH^{QM/MM}$	$g_1 = 2.01$ $g_2 = 2.04$ $g_3 = 2.07$	$Fe_p = 3.82$ $Fe_d = 27.51$	$Fe_p = 0.16$ $Fe_d = 0.88$
Exp.	$g_1 = 2.00$ $g_2 = 2.04$ $g_3 = 2.10$	$Fe_p = 12.4$ $Fe_d = 12.4$	- -

Table 5. *g* factors, hyperfine couplings and Mulliken spin populations calculated at the B3LYP/TZVP level on H_{ox} models **3**. Experimental data are also included.[21]

Model Name	*g* factors	Hyperfine couplings (MHz)	Mulliken spin pop.
3-$Fe_6S_6^{BS1}$	$g_1 = 2.02$ $g_2 = 2.06$ $g_3 = 2.07$	$Fe_p = 16.55$ $Fe_d = 24.69$	$Fe_p = 0.38$ $Fe_d = 0.63$
3-$Fe_6S_6^{BS2}$	$g_1 = 1.97$ $g_2 = 2.03$ $g_3 = 2.06$	$Fe_p = 15.52$ $Fe_d = 23.51$	$Fe_p = 0.36$ $Fe_d = 0.60$
3-$Fe_2S_2^{TRUNC}$	$g_1 = 2.01$ $g_2 = 2.05$ $g_3 = 2.05$	$Fe_p = 22.81$ $Fe_d = 20.77$	$Fe_p = 0.48$ $Fe_d = 0.51$
3-Fe_2S_2_AA	$g_1 = 2.01$ $g_2 = 2.03$ $g_3 = 2.04$	$Fe_p = 18.66$ $Fe_d = 21.14$	$Fe_p = 0.44$ $Fe_d = 0.52$
3-$DdH^{QM/MM}$	$g_1 = 2.01$ $g_2 = 2.05$ $g_3 = 2.05$	$Fe_p = 15.62$ $Fe_d = 25.09$	$Fe_p = 0.38$ $Fe_d = 0.64$
Exp.	$g_1 = 2.00$ $g_2 = 2.04$ $g_3 = 2.10$	$Fe_p = 12.4$ $Fe_d = 12.4$	- -

4. Corrections to the BS solutions. In the group of Neese, the performance of the BS approach for predicting EPR parameters of tetranuclear manganese complexes has been studied.[24] It was shown that the BS approach reproduces the electron density of the system of coupled spins correctly, while the obtained spin densities and thus the EPR parameters could be incorrect. The fact that Fe_6S_6 models result in almost the same hyperfine coupling constants as Fe_2S_2 models shows that BS DFT predicts "intrinsic" hyperfine coupling constants rather than the “effective” ones.[24]

Pantazis et al[24] have presented an approach to use BS states to calculate exchange-coupling constants. The solution of the Heisenberg exchange Hamiltonian, constructed from the obtained exchange-coupling constants, allows the calculation of on-site expectation values $\langle S_{Zi} \rangle$, which in turn represent correction coefficients that connect BS calculated hyperfine coupling constants with "true" estimates that could be compared with experiment. This approach has been shown to reproduce Mn hyperfine coupling constants rather well. Based on this approach, the scaling factors for the $^{57}Fe/^{13}C$ hyperfine couplings of the $[2Fe]_H$ subcluster are approximately 0.51, 0.89 and 0.38 for H_{ox}-CO, H_{ox} and H_{ox}-H_2O models, respectively (using the following estimates: $J_{cube} = 408$, 406 and 370 cm^{-1} for H_{ox}-CO, H_{ox} and H_{ox}-H_2O models, respectively; $J_H = 214$, 51 and 425 cm^{-1} for the same models). These scaling factors are definitely not enough to bring calculated values for models of the **1** and **2** types to the same level with experimental data. For models of the **3** type, the use of the scaling factor would make the Fe_p and Fe_d hyperfine couplings significantly lower than the experimental counterparts.

Table 6. *g* factors, hyperfine couplings and Mulliken spin populations calculated at the BP86/TZVP level on H_{ox} models **3**. Experimental data are also included.[21]

Model Name	*g* factors	Hyperfine couplings (MHz)	Mulliken spin pop.
3-$Fe_6S_6^{BS1}$	$g_1 = 2.00$ $g_2 = 2.03$ $g_3 = 2.06$	$Fe_p = 12.21$ $Fe_d = 19.72$	$Fe_p = 0.37$ $Fe_d = 0.63$
3-$Fe_6S_6^{BS2}$	$g_1 = 2.00$ $g_2 = 2.02$ $g_3 = 2.05$	$Fe_p = 10.74$ $Fe_d = 17.41$	$Fe_p = 0.32$ $Fe_d = 0.55$
3-$Fe_2S_2^{TRUNC}$	$g_1 = 2.01$ $g_2 = 2.02$ $g_3 = 2.04$	$Fe_p = 15.94$ $Fe_d = 18.14$	$Fe_p = 0.41$ $Fe_d = 0.59$
3-Fe_2S_2_surr	$g_1 = 2.01$ $g_2 = 2.02$ $g_3 = 2.03$	$Fe_p = 14.08$ $Fe_d = 17.55$	$Fe_p = 0.41$ $Fe_d = 0.54$
3-$DdH^{QM/MM}$	$g_1 = 2.00$ $g_2 = 2.02$ $g_3 = 2.04$	$Fe_p = 11.93$ $Fe_d = 19.81$	$Fe_p = 0.37$ $Fe_d = 0.62$
Exp.	$g_1 = 2.00$ $g_2 = 2.04$ $g_3 = 2.10$	$Fe_p = 12.4$ $Fe_d = 12.4$	- -

Conclusions

In the present contribution, we described a theoretical investigation of the magnetic properties of the H-cluster, using both simple Fe_2S_2 models and Fe_6S_6 models of the H-cluster, the latter in the context of broken-symmetry calculations. The protein environment has been modelled by different alternative approaches, viz. (i) extension of the QM region to the relevant amino-acids surrounding the Fe_2S_2 subsite of the H-cluster; (ii) a continuum solvent model with $\varepsilon = 40$, and (iii) an all-atom representation of the enzyme in the context of hybrid QM/MM modelling. The computed *g* factors of the CO-inhibited form of the enzyme turned out to be closer to experimental findings in the case of Fe_6S_6 models of the entire H-cluster optimized using the QM/MM approach. However, it is unclear if the accurate reproduction of the effects of the environment is actually beneficial for computation of the magnetic properties of the H-cluster at the level of theory here employed. In fact, for the H_{ox} state, the inclusion of the H-cluster surrounding in the model did not improve the computed *g* factors. Very similar conclusions can be drawn for the inclusion of the Fe_4S_4 subsite in the QM treatment: For example, for the H_{ox} state, the B3LYP results present large instability when one varies the BS coupling in the tetranuclear subcluster. Moreover, substantial differences in computed *g* values are observed also when one varies the density functional (BP86 vs. B3LYP). Large discrepancies in the computed *g* values were observed also in previous papers,[14, 19] as a function of the level of theory and of the composition of the model. This behaviour may be related to the spin–orbit coupling, a feature that greatly complicates their theoretical treatment.

A larger consistency of results is observed in the case of hyperfine coupling calculation, which are more localised parameters and consequently their prediction is more straightforward. In this regard, we show that the accuracy of the theoretical results is rather low in absolute terms, but the ratio between Fe_p and Fe_d couplings is well reproduced for the H_{ox}-CO state, the structure of which has been well characterized during the latest ten years.[3, 6, 14] More specifically, hyperfine couplings computed at BP86 level are almost independent of the extension of the QM model.

For the partially oxidized H_{ox} state, keeping in mind the above mentioned shortcomings of EPR parameters calculations, we can conclude that, in general, the theoretical *g* factors of H_{ox} models for both Fe_6S_6 and Fe_2S_2 support the hypothesis of a vacant coordination site trans to the bridging CO on Fe_d. However, the hyperfine coupling constants and thus the distribution of the spin density in the binuclear subcluster are closer to the experiment when a water ligand is present at the external site. Therefore, on the basis of the obtained data, we cannot reject any of these two models. However, as theoretical hyperfine couplings are expected to be more reliable than computed *g* factors, we are inclined to the model of the H_{ox} state with an attached water ligand (H_{ox}-H_2O). Previous results have pointed in the direction of a small affinity of the H-cluster towards H_2O.[25] However, if one admits that a water molecule can reach the cavity in front of the distal iron atom, one can propose that the formation of a hydrogen bond between the DTMA amine group and H_2O would bring the water oxygen atom in the vicinity of the Fe_d ion itself, a weak interaction that would have significant impact on the electronic properties of the binuclear cluster.

We believe that future efforts should be devoted to the development of a theoretical framework that is suitable for more accurate hyperfine coupling calculations of hydrogenases enzymes.

Methodological Section

Geometry optimizations of purely QM Fe_6S_6 models (**1-$Fe_6S_6^{BS1}$**, **1-$Fe_6S_6^{BS2}$**, **2-$Fe_6S_6^{BS1}$**, **2-$Fe_6S_6^{BS2}$**, **3-$Fe_6S_6^{BS1}$**, **3-$Fe_6S_6^{BS2}$**) were carried out using TURBOMOLE program suite,[26] at the BP86/TZVP level,[27] and making use of the resolution-of-identity (RI) technique.[28] The energy differences reported in the present paper were computed at such level of theory. In the optimization of the Fe_6S_6 models, all the cysteine alpha carbon atoms were constrained at their crystallographic positions,[1] and the COSMO continuum solvent model[16] was used, with a dielectric constant $\varepsilon = 40$. Such a dielectric constant turned out to best reproduce the CO-bridged geometry expected for the H_{ox} form of the enzyme, based on crystallographic data. From these optimized geometries, truncated models of the H-cluster were also obtained (**1-$Fe_2S_2^{TRUNC}$**, **2-$Fe_2S_2^{TRUNC}$**, **3-$Fe_2S_2^{TRUNC}$**), by substituting their $[Fe_4S_4](SCH_3)_3$ fragment with a hydrogen atom. In all cases, this hydrogen atom was bonded to the cysteine sulphur atom belonging to Fe_p coordination sphere. The S–H bond was assigned a 1.3 Å distance in all models.

At the next level of approximation, models of nine amino acids surrounding the Fe_2S_2 cluster were included (see Figure S1 in the Supplementary Material). The atomic composition and initial geometry of these models were obtained as described previously.[17] These models underwent constrained geometry optimizations in the COSMO continuum solvent at $\varepsilon = 40$. The constrained atoms are specified in the Supplementary Material (Figure S1).

As for the optimization of the QM/MM models, the COMQUM program was used,[29] and the approach already described by us was applied,[25] with the only difference that all calculations have been carried out using the large TZVP basis, in place of the smaller SVP basis used in our previous study. More generally, all the SCF calculation performed along the geometry optimizations here described were carried out at BP86-RI/TZVP level, using the broken-symmetry approach[23] in the case of Fe_6S_6 models (see Supplementary Material for details on spin distributions in the BS1 and BS2 wavefunctions, Figure S3. These two electronic states present opposite spin localization patterns on the Fe_4S_4 subcluster, while the α-spin excess on the binuclear subcluster is always left unaltered. Thus, both the possible cases of ferromagnetic and antiferromagnetic coupling between the Fe_2S_2 subsite and the closest Fe atom in the Fe_4S_4 moiety are taken into account here). To obtain broken-symmetry wavefunctions featuring specific patterns of spin excess on the H-cluster tetranuclear subsite, we applied an approach recently described by us [add Greco et al, International Journal of Quantum Chemistry, in press].

DFT calculations of *g* factors and hyperfine couplings was carried out using the ORCA 2.6 program [add ref ORCA], both at the BP86-RI/TZVP and the B3LYP/TZVP level.[30]

Supporting Information (see footnote on the first page of this article): … . Describe supporting info content

Acknowledgments

C. G. Acknowledges support from Humboldt Foundation

References at the end of the present document

Received: ((will be filled in by the editorial staff))
Published online: ((will be filled in by the editorial staff))

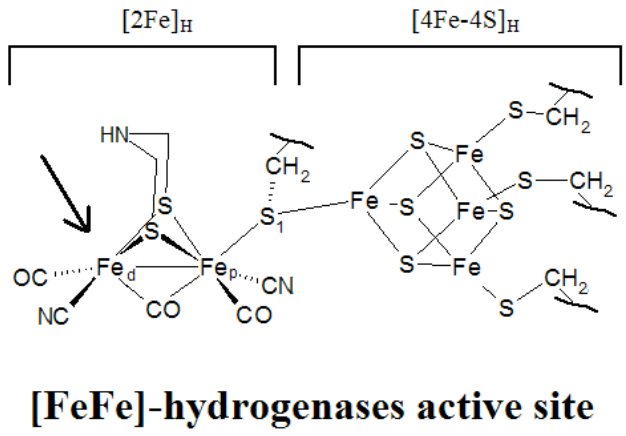

Figure 1. Schematic representation of the H-cluster

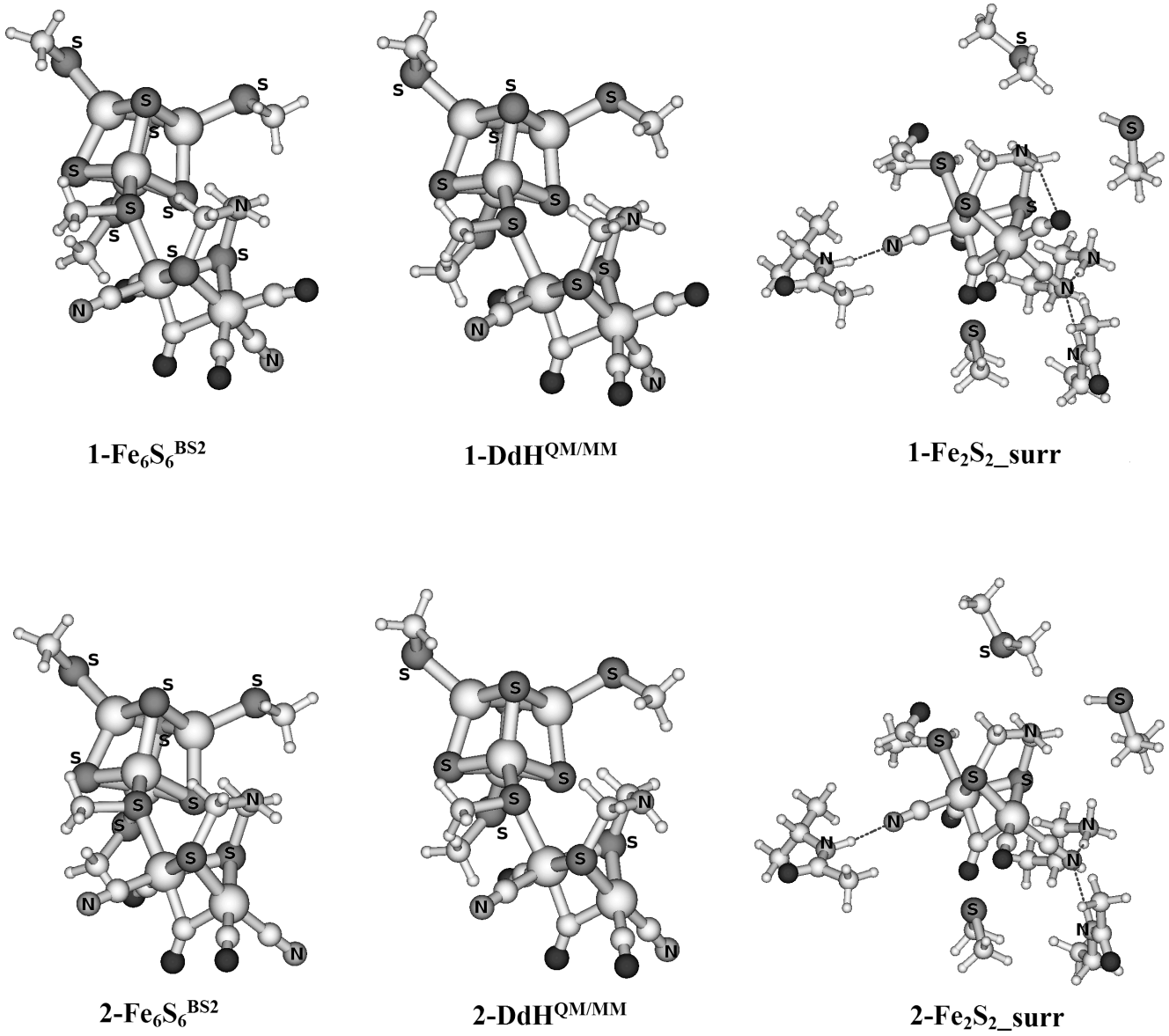

Figure 2: Upper row: geometries of models **1-Fe$_6$S$_6^{BS1}$**, **1-DdH$^{QM/MM}$** and **1-Fe$_2$S$_2$_surr**. Notice that the CH_3SH fragment representing Cys178 (see Methods), which belongs to the QM region of both the QM/MM models **1-DdH$^{QM/MM}$** and **2-DdH$^{QM/MM}$**, has been omitted in the present pictorial representation, for the sake of clarity. Small, middle-size and large white spheres correspond to hydrogen, carbon and iron atoms, respectively; dark grey, middle-size spheres represent oxygen atoms.

Supporting Information

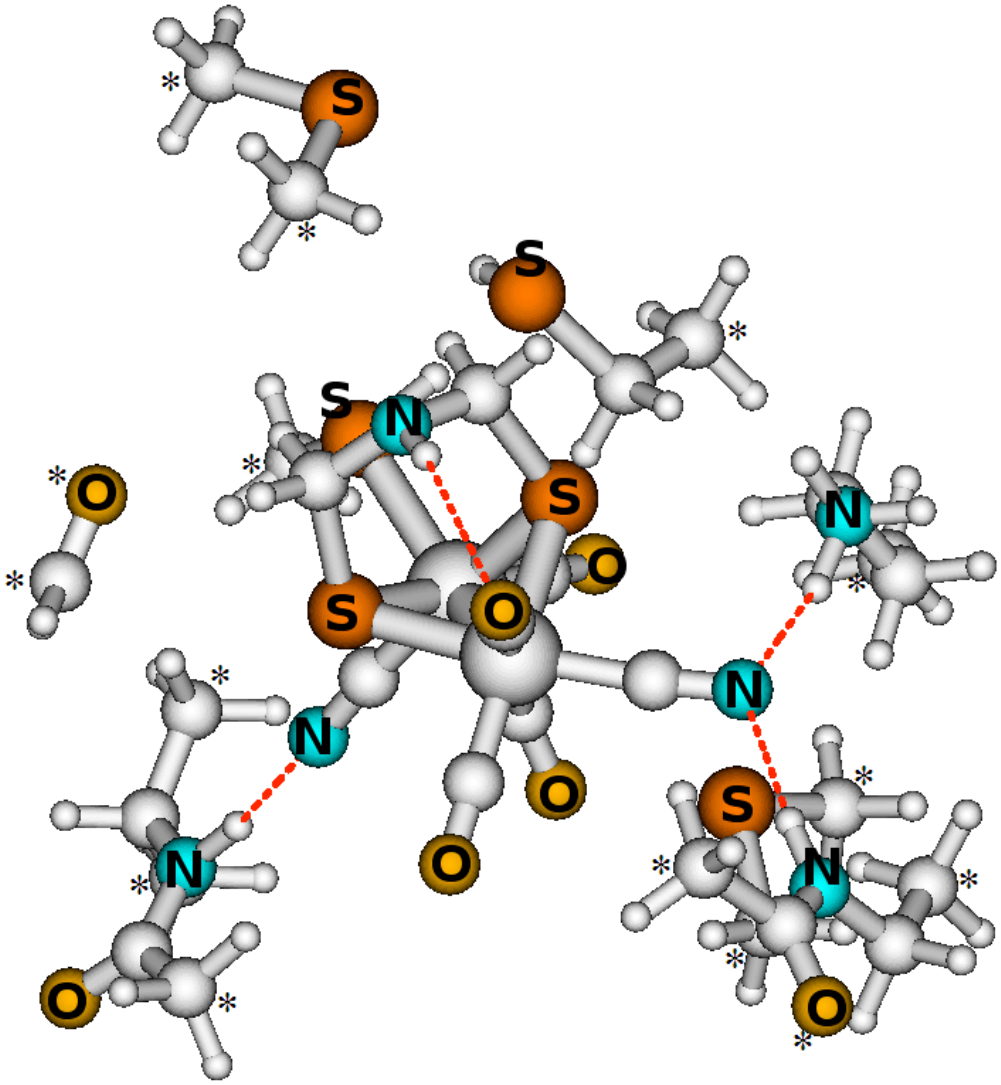

Figure S1. Atoms that were kept at the crystallographic position in models of the Fe_2S_2 subsite with fragments of the surrounding amino acids. The atoms fixed in space (in all cases either oxygen or carbon atoms) are indicated with an asterisk. Small, middle-size and large white spheres correspond to hydrogen, carbon and iron atoms, respectively. **Xxx Colours.**

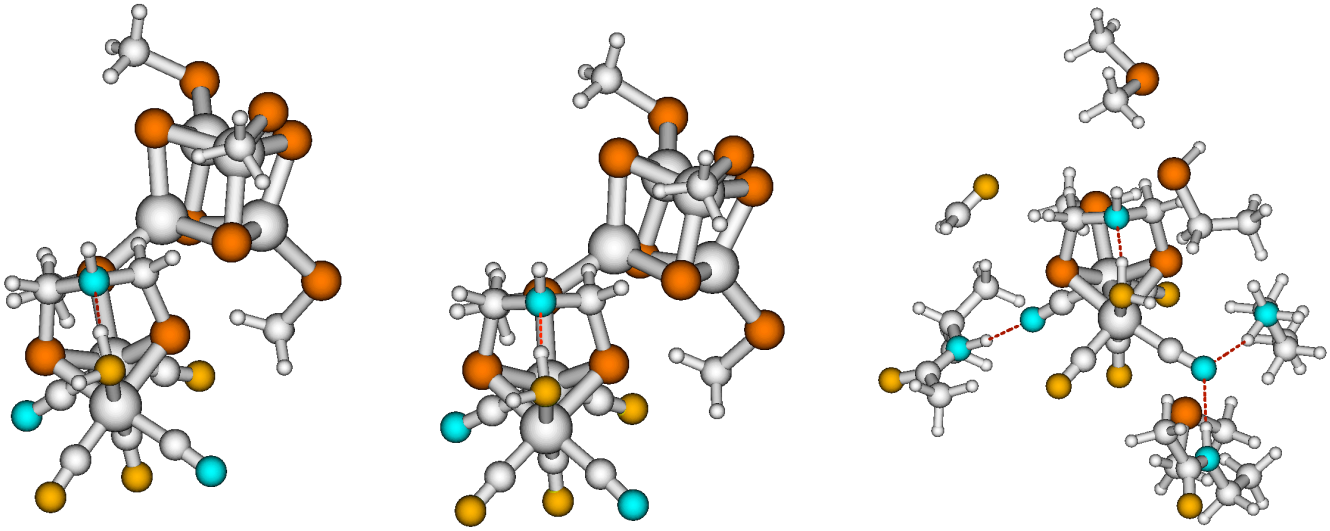

Figure S2. Geometries of models **3-Fe$_6$S$_6$^{BS1}**, **3-DdH$^{QM/MM}$** and **3-Fe$_2$S$_2$_surr**. Notice that the CH_3SH fragment representing Cys178 (see Methods), which belongs to the QM region of both the QM/MM model **3-DdH$^{QM/MM}$**, has been omitted in the present pictorial representation, for the sake of clarity. The colour code used for the various elements is the same as in Figure S1.

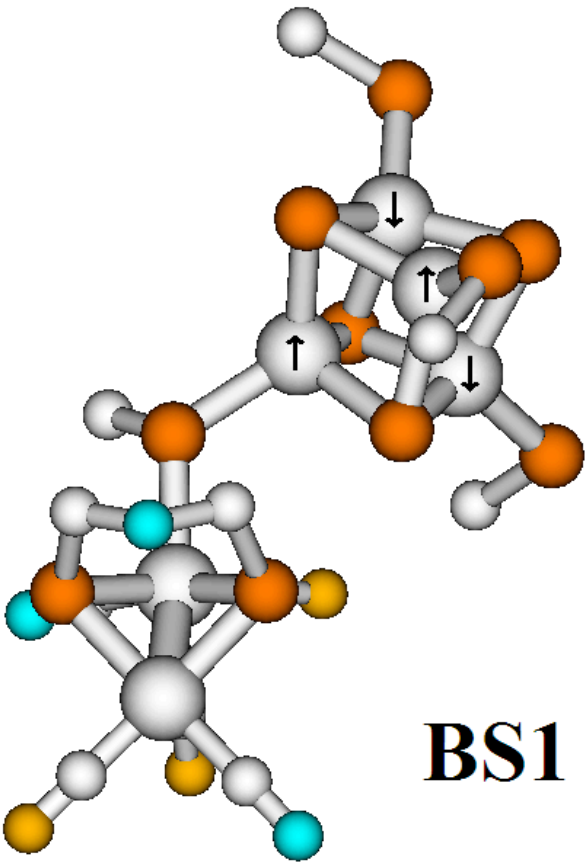

Figure S3. Schematic representation of the spin-excess pattern of the BS1-type broken-symmetry wavefunction. Arrows pointing up and down indicate alpha and beta spin excess, respectively. In the BS2 coupling scheme, the localization of alpha and beta spin excesses are inverted. Hydrogen atoms have been omitted for clarity; for the remaining atoms, the colour code used is the same as in Figure S1.

References:

[1] Y. Nicolet, C. Piras, P. Legrand, C. E. Hatchikian and J. C. Fontecilla-Camps, *Structure with Folding & Design* **1999**, *7*, 13-23.
[2] J. W. Peters, W. N. Lanzilotta, B. J. Lemon and L. C. Seefeldt, *Science* **1998**, *282*, 1853-1858; A. S. Pandey, T. V. Harris, L. J. Giles, J. W. Peters and R. K. Szilagyi, *Journal of the American Chemical Society* **2008**, *130*, 4533-4540.
[3] B. J. Lemon and J. W. Peters, *Biochemistry* **1999**, *38*, 12969-12973.
[4] Y. Nicolet, A. L. de Lacey, X. Vernede, V. M. Fernandez, E. C. Hatchikian and J. C. Fontecilla-Camps, *Journal of the American Chemical Society* **2001**, *123*, 1596-1601.
[5] W. Roseboom, A. L. De Lacey, V. M. Fernandez, E. C. Hatchikian and S. P. J. Albracht, *Journal of Biological Inorganic Chemistry* **2006**, *11*, 102-118.
[6] Z. J. Chen, B. J. Lemon, S. Huang, D. J. Swartz, J. W. Peters and K. A. Bagley, *Biochemistry* **2002**, *41*, 2036-2043.
[7] A. Silakov, C. Kamp, E. Reijerse, T. Happe and W. Lubitz, *Biochemistry* **2009**, *48*, 7780-7786.
[8] Z. X. Cao and M. B. Hall, *Journal of the American Chemical Society* **2001**, *123*, 3734-3742.
[9] W. Lubitz, E. Reijerse and M. van Gastel, *Chemical Reviews* **2007**, *107*, 4331-4365.
[10] A. S. Pereira, P. Tavares, I. Moura, J. J. G. Moura and B. H. Huynh, *Journal of the American Chemical Society* **2001**, *123*, 2771-2782; C. V. Popescu and E. Munck, *Journal of the American Chemical Society* **1999**, *121*, 7877-7884.
[11] M. Bruschi, C. Greco, G. Zampella, U. Ryde, C. J. Pickett and L. De Gioia, *Comptes Rendus Chimie* **2008**, *11*, 834-841; H. J. Fan and M. B. Hall, *Journal of the American Chemical Society* **2001**, *123*, 3828-3829.
[12] P. E. M. Siegbahn, J. W. Tye and M. B. Hall, *Chemical Reviews* **2007**, *107*, 4414-4435.
[13] S. P. J. Albracht, W. Roseboom and E. C. Hatchikian, *Journal of Biological Inorganic Chemistry* **2006**, *11*, 88-101.
[14] C. Greco, M. Bruschi, J. Heimdal, P. Fantucci, L. De Gioia and U. Ryde, *Inorganic Chemistry* **2007**, *46*, 7256-7258.
[15] M. Bruschi, C. Greco, P. Fantucci and L. De Gioia, *Inorganic Chemistry* **2008**, *47*, 6056-6071.
[16] A. Klamt, *Journal of Physical Chemistry* **1995**, *99*, 2224-2235.
[17] A. Silakov, B. Wenk, E. Reijerse and W. Lubitz, *Physical Chemistry Chemical Physics* **2009**, *11*, 6592-6599.
[18] A. Silakov, B. Wenk, E. Reijerse, S. P. J. Albracht and W. Lubitz, *Journal of Biological Inorganic Chemistry* **2009**, *14*, 301-313.
[19] A. T. Fiedler and T. C. Brunold, *Inorganic Chemistry* **2005**, *44*, 9322-9334.
[20] M. van Gastel, C. Fichtner, F. Neese and W. Lubitz, *Biochemical Society Transactions* **2005**, *33*, 7-11.
[21] A. Silakov, E. J. Reijerse, S. P. J. Albracht, E. C. Hatchikian and W. Lubitz, *Journal of the American Chemical Society* **2007**, *129*, 11447-11458.
[22] D. E. Schwab, C. Tard, E. Brecht, J. W. Peters, C. J. Pickett and R. K. Szilagyi, *Chemical Communications* **2006**, 3696-3698.
[23] L. Noodleman and J. G. Norman, *Journal of Chemical Physics* **1979**, *70*, 4903-4906; L. Noodleman, *Journal of Chemical Physics* **1981**, *74*, 5737-5743.
[24] D. A. Pantazis, M. Orio, T. Petrenko, S. Zein, E. Bill, W. Lubitz, J. Messinger and F. Neese, *Chemistry-a European Journal* **2009**, *15*, 5108-5123.
[25] C. Greco, M. Bruschi, L. De Gioia and U. Ryde, *Inorganic Chemistry* **2007**, *46*, 5911-5921.
[26] R. Ahlrichs, M. Bar, M. Haser, H. Horn and C. Kolmel, *Chemical Physics Letters* **1989**, *162*, 165-169.
[27] A. D. Becke, *Physical Review A* **1988**, *38*, 3098-3100; J. P. Perdew, *Physical Review B* **1986**, *33*, 8822-8824; A. Schafer, C. Huber and R. Ahlrichs, *Journal of Chemical Physics* **1994**, *100*, 5829-5835.

[28] K. Eichkorn, O. Treutler, H. Ohm, M. Haser and R. Ahlrichs, *Chemical Physics Letters* **1995**, *240*, 283-289; K. Eichkorn, F. Weigend, O. Treutler and R. Ahlrichs, *Theoretical Chemistry Accounts* **1997**, *97*, 119-124.
[29] U. Ryde, *Journal of Computer-Aided Molecular Design* **1996**, *10*, 153-164; U. Ryde and M. H. M. Olsson, *International Journal of Quantum Chemistry* **2001**, *81*, 335-347.
[30] A. D. Becke, *Journal of Chemical Physics* **1993**, *98*, 5648-5652; C. T. Lee, W. T. Yang and R. G. Parr, *Physical Review B* **1988**, *37*, 785-789.